2009 American Control Conference
Hyatt Regency Riverfront, St. Louis, MO, USA
June 10-12, 2009

Detection of Local Stiffness and Piezoelectric Properties of Materials via Piezoresponse Force Microscopy

Amin Salehi-Khojin, Saeid Bashash, Nader Jalili, Gary Lee Thompson, and Alexey Vertegel

Abstract—**The objective of this study is to propose a practical framework for simultaneous estimation of the local stiffness and piezoelectric properties of materials via piezoresponse force microscopy (PFM). For this, the governing equation of motion of a vertical PFM is derived at a given point on the sample. Using the expansion theorem, the governing ordinary differential equations (ODEs) of the system and their state-space representation are derived under applied external voltage. For the proof of the concept, the results obtained from both frequency and step responses of a PFM experiment are utilized to simultaneously identify the microcantilever parameters along with local spring constant and piezoelectric coefficient of a Periodically Poled Lithium Niobate (PPLN) sample. In this regard, a new parameter estimation strategy is developed for modal identification of system parameters under general frequency response. Results indicate good agreements between the identified model and the experimental data using the proposed modeling and identification framework.**

I. INTRODUCTION

Piezoelectric materials are one of the most promising materials which have attracted a lot of attention since their discovery in the 19th century [1-3]. Ever since many works have been carried out in developing applications for piezoelectric materials in micro-electromechanical systems (MEMS) [4 and 5] due to their high sensitivity and low electrical noise in sensing applications and high output force in actuators compared to other conventional designs.

However, to implement piezoelectric materials in micro- and nano-scale structures, the study of size effect in low dimensional structures is a crucial step. It has been shown that as the dimension of piezoelectric materials reduces to microscopic levels, they cannot preserve their macroscopic properties, and a significant deviation is observed when compared to bulk materials [6]. In this respect, characterization of material in low-dimensional scales requires different technique than those utilized for bulk materials.

Piezoresponse force microscopy (PFM) has attracted widespread attention as a primary technique for nondestructive characterization of piezoelectric materials in the grain scale [7-11]. PFM functions based on a periodic bias electrical field applied between an electrode on the rear side of piezoelectric sample and a conducting AFM tip. The piezoresponse of the surface can be detected from the harmonic component of the tip deflection in which the amplitude of vibration can provide information on the piezoelectric coefficients of surface [11 and 12].

Recently, comprehensive models for dynamic behavior of vector PFM system with coupled motions have been introduced [13 and 14]. The PFM system has been modeled as a suspended microcantilever in contact with a material through a small tip. For the purpose of modeling, the material was considered to exhibit piezo-elastic [13] or piezo-viscoelastic [14] behavior in all directions. The results have addressed the contribution of coupled mode on the vibration spectra of the other modes for very stiff materials [14]. However, the contribution of coupling terms for regular and soft materials has been shown to be negligible. Despite of all these studies, there is a lack of experimental vibration analysis and validation of PFM for a given frequency domain data. Particularly, the local spring constant of sample can only be obtained from the modal analysis of system. Otherwise, the theory of contact mechanics based on the exact geometry of tip/sample interaction must be utilized which is difficult in practice.

The objective of this study is to use modal analysis of vertical PFM for low dimensional material characterization purpose. In this regard, the governing equation of motion is obtained for vertical PFM at a given point on the sample. The modal analysis is carried out and the governing ordinary differential equations (ODEs) of system and its state-space representation are derived under applied external voltage. The proposed model is then experimentally implemented to identify local stiffness and piezoelectric coefficient of a Periodically Poled Lithium Niobate (PPLN) sample. Due to the non-homogeneities and uncertainties in the microcantilever parameters, a new system identification strategy is implemented to simultaneously detect the experimental resonances associated with the vertical modes and identify the uncertain microcantilever and sample parameters. Results indicate successful convergence of modeling error for the acquired experimental data. The proposed strategy can be useful for accurate characterization of biological species with piezoelectric properties.

A. Salehi-Khojin, S. Bashash and N. Jalili are with the Smart Structures and Nanoelectromechanical Systems Laboratory, Department of Mechanical Engineering, Clemson University, Clemson, SC 29634, USA (N. Jalili is associate professor and the corresponding author, phone: 864-656-5642; fax: 864-656-4435; e-mail: jalili@clemson.edu).

G. L. Thomson, and A. Vertegel are with the Department of Bioengineering, Clemson University, Clemson, SC 29634, USA.

978-1-4244-4524-0/09/$25.00 ©2009 AACC

II. Distributed-Parameters Modeling of PFM

A PFM system can be modeled as a microcantilever beam with linear density ρ and rigidity EI, clamped to a movable base from one side, and in contact with a piezoelectric material on the other side through a small tip with mass m_e (see Fig. 1). When the external electric field is applied between the conducting tip and sample, the response of material can be divided into viscoelastic and piezoelectric parts. The viscoelastic part can be modeled based on Kelvin-Voigt model (parallel spring and damper), while the piezoresponse of material can be considered as a force acting on the tip given by $F_{tip}(t) = \gamma V(t)$, where γ and $V(t)$ represent the piezoelectric coefficient of material and the applied voltage, respectively.

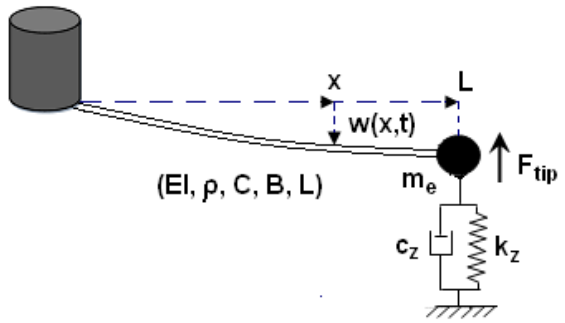

Fig. 1. A schematic model of vertical PFM and sample.

Using the extended Hamilton's Principle and following the same procedure as outlined in [14], the partial differential equation (PDE) for the transversal vibration of microcantilever in the absence of base motion, which is our case of interest (the point scanning problem), can be expressed as:

$$\rho w_{tt}(x,t) + EIw_{xxxx}(x,t) + Bw_t(x,t) + Cw_{xt}(x,t) = 0 \quad (1)$$

with the following boundary conditions:

$$\begin{aligned} w(0,t) = w_x(0,t) = w_{xx}(L,t) = 0 \\ m_e w_{tt}(L,t) - EIw_{xxx}(L,t) + k_z w(L,t) + C_z w_t(L,t) = F_{tip}(t) \end{aligned} \quad (2)$$

In the above equations, subscripts $(\cdot)_t$ and $(\cdot)_x$ indicate the partial derivatives with respect to the time variable t and spatial variable x, respectively. B and C are the respective viscous and structural damping coefficients of cantilever, k_z is the spring constant, and C_z is the damping coefficient of material.

To derive the truncated ordinary differential equations (ODEs) of system, the modal and forced motion analyses are carried out in the next sections.

III. System Modal Analysis

In order to obtain natural frequencies and mode shapes of the system, the eigenvalue problem associated with the transversal vibration of microcantilever is obtained by applying free and un-damped conditions to Eqs. (1) and (2) which results in:

$$\rho w_{tt}(x,t) + EIw_{xxxx}(x,t) = 0 \quad (3)$$

with the following boundary conditions:

$$\begin{aligned} w(0,t) = w_x(0,t) = 0 \\ w_{xx}(L,t) = m_e w_{tt}(L,t) - EIw_{xxx}(L,t) + k_z w(L,t) = 0 \end{aligned} \quad (4)$$

The solution to $w(x,t)$ can be assumed in the following separable form:

$$w(x,t) = \Phi(x)e^{i\omega t} \quad (5)$$

where $\Phi(x)$ is the modal displacement function and ω is the natural frequency of system. Inserting Eq. (5) into Eq. (3), the general solution of the modal displacement function can be expressed as:

$$\Phi(x) = K_1[\sin(\lambda x) - \sinh(\lambda x)] + K_2[\cos(\lambda x) - \cosh(\lambda x)] \quad (6)$$

where K_1 and K_2 are constant coefficients and $\lambda = \left(\rho\omega^2 / EI\right)^{1/4}$.

Substituting Eq. (6) into the free and undamped boundary conditions at $x = L$ (the second line of Eq. (4)) results in following characteristics matrix equation:

$$\begin{bmatrix} A_{11} & A_{12} \\ A_{21} & A_{22} \end{bmatrix} \begin{bmatrix} K_1 \\ K_2 \end{bmatrix} = 0 \quad (7)$$

where

$$\begin{aligned} A_{11} &= EI\lambda^3\left(\cos\lambda L + \cosh\lambda L\right) + \\ &\quad \left(k_z - m_e\omega^2\right)\left(\sin\lambda L - \sinh\lambda L\right), \\ A_{12} &= -EI\lambda^3\left(\sin\lambda L - \sinh\lambda L\right) + \\ &\quad \left(k_z - m_e\omega^2\right)\left(\cos\lambda L - \cosh\lambda L\right), \\ A_{21} &= \sin\lambda L + \sinh\lambda L, \\ A_{22} &= \cos\lambda L + \cosh\lambda L \end{aligned} \quad (8)$$

Note that boundary conditions at $x = 0$ have been already included in the derivation of Eq. (6).

The frequency equation can now be obtained by equating the determinant of Eq. (7) to zero. This leads to determination of system natural frequencies. In order to determine the unique solution for the coefficients of mode shapes, $(K_1)_i$ and $(K_2)_i$, corresponding to the i^{th} natural frequency, the orthogonality condition of mode shapes (the normalization condition with respect to mass) is utilized which is given by:

$$\int_0^L \rho\phi_i(x)\phi_j(x)dx + m_e\phi_i(L)\phi_j(L) = \delta_{ij}, \quad i,j = 1,2,\ldots,\infty \quad (9)$$

where $\phi_i(x)$ and $\phi_j(x)$ are the i^{th} and j^{th} mode shapes of system, and δ_{ij} is the Kronecker delta. The obtained mode shapes are utilized in the forced vibration analysis of the system which is the focus of the study in the following section.

IV. Forced Motion Analysis of Microcantilever

Using expansion theorem for the beam vibration analysis, the expression for transversal displacement can be written as:

$$w(x,t)=\sum_{i=1}^{\infty}\phi_i(x)q_i(t) \tag{10}$$

where $q_i(t)$ are the generalized time-dependent coordinates. Inserting Eq. (10) into Eq. (1), multiplying both sides by $\phi_j(x)$, integrating over the length of the cantilever and using the orthogonality conditions given by:

$$\begin{aligned}&\int_0^L \rho\phi_i(x)\phi_j(x)dx+m_e\phi_i(L)\phi_j(L)=\delta_{ij}\\&\int_0^L EI\phi_i''(x)\phi_j''(x)dx+k_z\phi_i(L)\phi_j(L)=\omega_i^2\delta_{ij},\end{aligned} \tag{11}$$

the ODEs representing the forced vibration of system can be written as:

$$\ddot{q}_i(t)+\sum_{j=1}^{\infty}C_{ij}\dot{q}_j(t)+\omega_i^2q_i(t)=f_iV(t) \tag{12}$$

where

$$C_{ij}=\int_0^L\phi_i(x)\left[B\phi_i(x)+C\phi_j'(x)\right]dx+C_z\phi_i(L)\phi_j(L),\quad f_i=\gamma\phi_i(L) \tag{13}$$

The truncated *n*-mode description of the beam Eq. (12) can now be presented in the following matrix form:

$$\mathbf{M}\ddot{\mathbf{q}}+\mathbf{C}\dot{\mathbf{q}}+\mathbf{K}\mathbf{q}=\mathbf{F}u \tag{14}$$

where

$$\begin{aligned}&\mathbf{M}=I_{n\times n},\ \mathbf{C}=[C_{ij}]_{n\times n},\ \mathbf{K}=[\omega_i^2\delta_{ij}]_{n\times n},\\&\mathbf{q}=[q_1(t),q_2(t),\ldots,q_n(t)]_{n\times1}^T,\mathbf{F}=[f_1,f_2,\ldots,f_n]_{n\times1}^T,\ u=V(t)\end{aligned} \tag{15}$$

The state-space representation of Eq. (14) is given by:

$$\dot{\mathbf{X}}=\mathbf{A}\mathbf{X}+\mathbf{B}u \tag{16}$$

where

$$\mathbf{A}=\begin{bmatrix}\mathbf{0}&\mathbf{I}\\-\mathbf{M}^{-1}\mathbf{K}&-\mathbf{M}^{-1}\mathbf{C}\end{bmatrix}_{2n\times2n},\ \mathbf{B}=\begin{bmatrix}\mathbf{0}\\\mathbf{M}^{-1}\mathbf{F}\end{bmatrix}_{2n\times1},\ \mathbf{X}=\begin{Bmatrix}\mathbf{q}\\\dot{\mathbf{q}}\end{Bmatrix}_{2n\times1} \tag{17}$$

Once the system is represented in state-space, its frequency response can be plotted to demonstrate the behavior of system within a desired frequency range. Without loss of generality, the displacement of any arbitrary point (i.e., $x=L_0$) can be taken the system output as follows:

$$\begin{aligned}&\mathbf{Y}(t)=w(L_0,t)=\sum_{i=1}^{n}\phi_i(L_0)q_i(t)=\\&[\phi_1(L_0),\phi_2(L_0),\ldots,\phi_n(L_0),0,\ldots,0]_{1\times2n}\mathbf{X}(t)=\mathbf{C}_{L0}\mathbf{X}(t)\end{aligned} \tag{18}$$

The frequency response of the system can now be plotted using the transfer function obtained through the Laplace transformation of the state-space model as follows:

$$G(s)=\frac{Y(s)}{U(s)}=\mathbf{C}_{L0}(sI-\mathbf{A})^{-1}\mathbf{B} \tag{19}$$

In the next section, an experimental procedure is presented for validation of the proposed framework utilized for identification of piezomechanical properties of a real sample.

V. Experimental Procedure and Setup

In this study, a commercial AFM (Asylum Research MFP-3D) with an Au/Cr-coated SiN pyramidal tip on a triangular microcantilever (TR400PB, Olympus) are used for indentation of sample. The sample is periodically poled lithium niobate (PPLN), made by Crystal Technologies, Inc. using the electric-field poling technique [15, 16]. The tip is positioned on a c⁻ domain using the force panel in contact mode. At this location, the frequency of the voltage applied to the tip is swept from 0 Hz to 1 MHz. The resulting frequency response is depicted in Fig. 2.

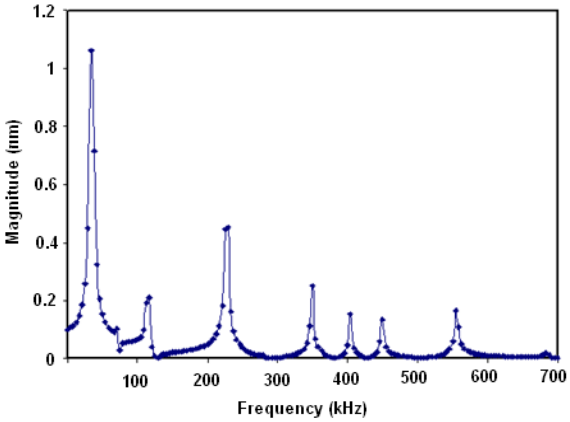

Fig. 2. Experimental frequency response plot of PPLN.

Due to uncertainties and non-homogeneities in the system, the resonant frequencies obtained from experimental frequency response could also include non-bending modes such as torsion. In order to investigate the possible presence of other modes, an experimental setup is built using a state-of-the-art microsystem analyzer, the MSA-400 manufactured by Polytec Incorporated. The MSA-400 employs the laser Doppler vibrometry and stroboscopic video microscopy to measure the 3D dynamic response of microcantilever (see Fig. 3). For this purpose, an input voltage of 10V is applied to a piezoelectric actuator at the base of microcantilever, and the 3D motion of microcantilever is studied at different resonant frequencies. It is observed that for the range of frequency swept from 0 to 1 MHz, the microcantilever operates at different modes other than bending. Fig. 4 depicts two examples of bending and mixed bending/torsion motions of microcantilever captured by MSA-400.

Since the mathematical vibration model presented in the previous section reflects only the vertical motion of system, the corresponding experimental resonant frequencies of

bending must be separated from non-bending modes. In this respect, the following section focuses on an optimization algorithm developed for this purpose.

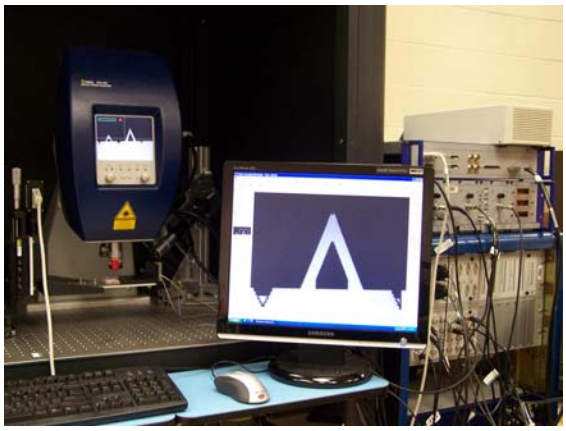

Fig. 3. Experimental setup for microcantilever under Micro System Analyzer (MSA-400).

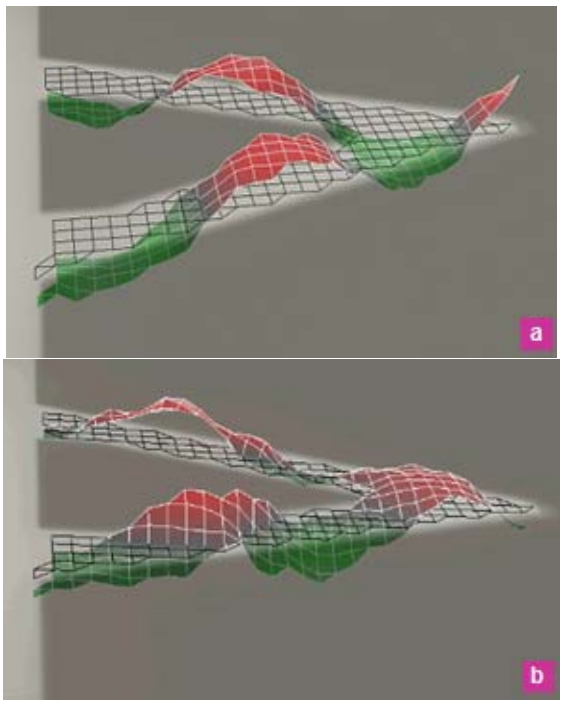

Fig. 4. Examples for 3D motion of triangular microcantilever at (a) pure bending, and (b) mixed bending/torsion motions.

VI. Modal System Identification and Material Characterization

In order to detect piezomechanical properties of PPLN based on the results obtain from theory and experiment, a system identification procedure is required to characterize the entire system parameters. For this purpose, the experimental frequency response of system is utilized for the identification of system parameters. From the sharp peaks of experimental frequency response (Fig. 2), one can choose the system natural frequencies approximately equal to the system resonant frequencies. This is due to the fact that resonant and natural frequencies are very close for systems with low damping ratios. Hence, frequency response peaks can be used for the identification of parameters associated with free and undamped system. From the equation of motion and boundary conditions, the independent parameters to be identified include both cantilever parameters and the local spring constant of material, which are 4 unknowns forming independent parameters' vector $P=\left[\rho/EI, m_e/EI, k_z/EI, L\right]$.

Since the mathematical model developed in Sections 3 and 4 reflects only the vertical vibration mode of microcantilever and the experimental frequency response contains all the resonant modes including vertical and non-vertical modes within the swept frequency range, an efficient method is required to extract the experimental vertical modes and use them for accurate estimation of system parameters. Here, a double optimization technique has been developed and utilized to identify system under an uncertain frequency response. For the 4 unknown parameters of system, at least 4 vertical resonant frequencies are needed for the system identification. To add more safety, the first 5 resonant frequencies are selected here. Since the first 5 peaks of experiment may include non-vertical modes, we have chosen first 10 resonances of experiment so that they certainly include all the first 5 vertical modes. Hence, the system identification objective selected here is to minimize the error between the model and experimental frequency responses under initially uncertain system parameters and experimental data.

In general, assume that there are N chosen experimental resonances from which M ($M<N$) vertical peaks must be detected. Therefore, the total number of possible combinations of M frequencies from a set of N options is:

$$\binom{N}{M}=\frac{N!}{M!\times(N-M)!} \tag{20}$$

In every optimization step, the error between the model (with M modes) and all the possible experimental frequency sets are calculated individually. Then, the one with the minimum error value is selected as the best set with the highest probability with its frequencies all being the vertical resonances. This probability may be low at the beginning, however, as the optimization process evolves, the overall identification error is minimized and the probabilities of choosing the correct resonances and estimating the accurate parameter values increase.

A random optimization algorithm is implemented for the parameters estimation using MATLAB programming software [17]. Fig. 5a shows the descending trajectory of the average error percentage during the optimization process. Fig. 5b demonstrates the evolution of selected experimental frequencies with respect to optimization iterations. As seen, at initial optimization steps, resonant frequencies of model search for their optimum positions; as the optimization proceeds, they converge to their optimal set, where the

identification error is the least. In the meantime, system parameters converge to their optimal solution. Table 1 shows the parameters' initial values, upper and lower bounds, and the final optimal values. For cantilever stiffness $EI = 5.33\times10^{-14}\left(N.m^2\right)$ provided by the manufacturer, the optimal value of local spring constant of PPLN is determined to be 44.2 N/m. The average error percentage decreases from 18% to 2% in 500 optimization iterations. Fig. 6 depicts the frequency response of identified model compared to the experimental resonances. It is clearly seen that how the experimental resonances associated with the non-bending modes can be detected and skipped by the algorithm based on the least error criterion.

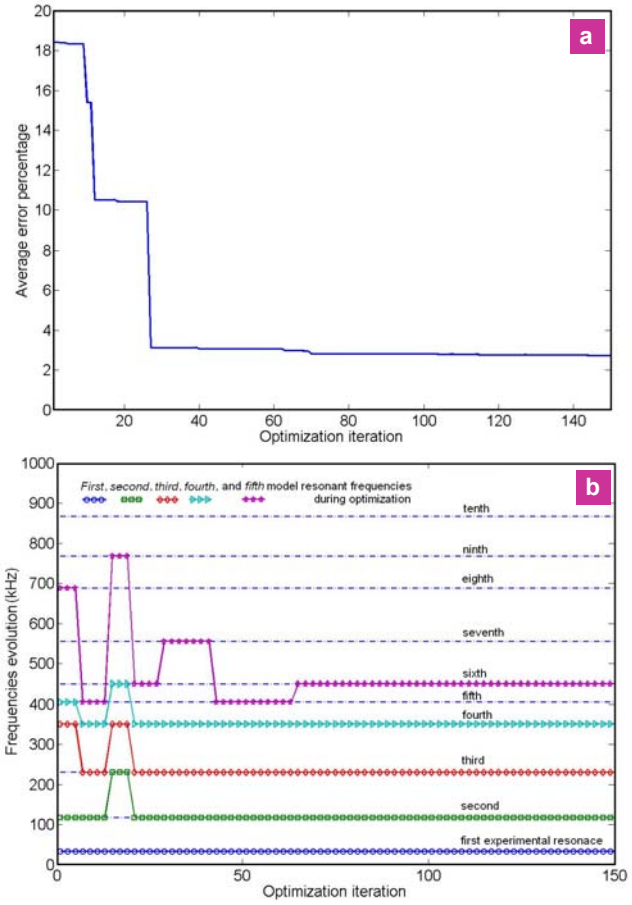

Fig. 5. (a) Average error percentage trajectory in random optimization, (b) evolution of selected frequencies associated with the transversal motion.

In order to obtain the piezoelectric coefficient of PPLN, a unit step input voltage with duration of 3 milliseconds is applied to the sample. The response of PPLN is demonstrated in Fig. 7. Since the equivalent spring constant in the tip-sample junction can be considered as a parallel combination of cantilever and material springs, the piezoelectric coefficient (γ) at tip-sample junction can be expressed as:

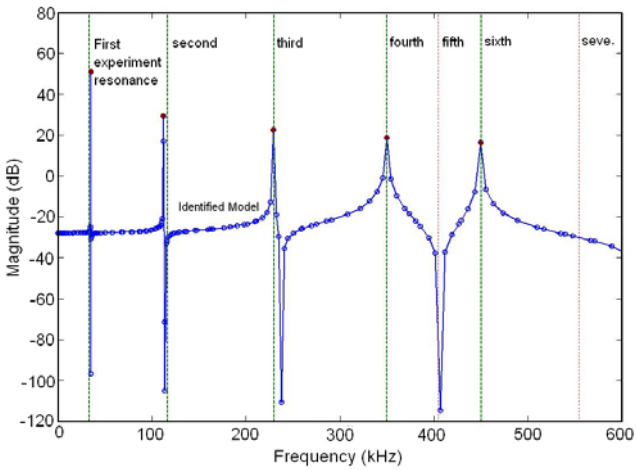

Fig. 6. Frequency response of the identified model compared to the experimental resonances.

Table 1. System parameters for system identification.

System parameters	Lower bound	Upper bound	Initial values	Optimal solution
ρ/EI $\left(kg/N.m^3\right)$	2×10^6	8×10^6	4×10^6	5.1×10^6
m_e/EI $\left(kg/N.m^2\right)$	10	200	50	110.3
k_z/EI $\left(1/m^3\right)$	0.5×10^{15}	5×10^{15}	2×10^{15}	0.83×10^{15}
$L(m)$	150×10^{-6}	250×10^{-6}	200×10^{-6}	176×10^{-6}

$$\gamma = (k_b + k_z)\frac{h}{V} \tag{21}$$

where the microcantilever spring is $k_b = 3EI/L^3$, k_z is the local spring constant of material obtained from frequency response, h is the steady-state (static) response of material to input voltage V. Using the optimal parameters of microcantilever and local spring constant of PPLN from Table 1, the piezoelectric coefficient of the PPLN (γ) is obtained as 2.54 (nN/V) which yields the standard piezoelectric coefficient d_{33}=57.4 (pm/V) determined by $d_{33} = \gamma/k_z$. Comparing the obtained values of d_{33} and the steady-state amplitude of unit step response demonstrate that the standard piezoelectric coefficient of materials can be directly estimated from the steady-state step response. This is due to the fact that the spring constant of microcantilever is negligible compared to that of the material in static mode.

VII. Conclusions

Utilizing a vertical PFM, a new procedure was introduced to estimate the local stiffness and piezoelectric properties of materials. It was shown that the dynamics of vertical PFM system can be governed by a partial differential equation (PDE) with clamped-viscoelastic boundary conditions. A

general formulation was then derived for the mode shape and frequency response of the system. Using the expansion theorem, the governing ordinary differential equations (ODEs) of the system and its state-space representation were derived under applied external voltage. Utilizing the frequency response of experiment and theory, the local spring constant of a piezoelectric material (i.e., PPLN) was obtained through minimizing the percentage of modeling errors. In this regard, a new parameter estimation technique was developed for modal identification of system parameters under an uncertain frequency response. Moreover, the experimental step response of system was used to estimate the standard piezoelectric coefficient of PPLN.

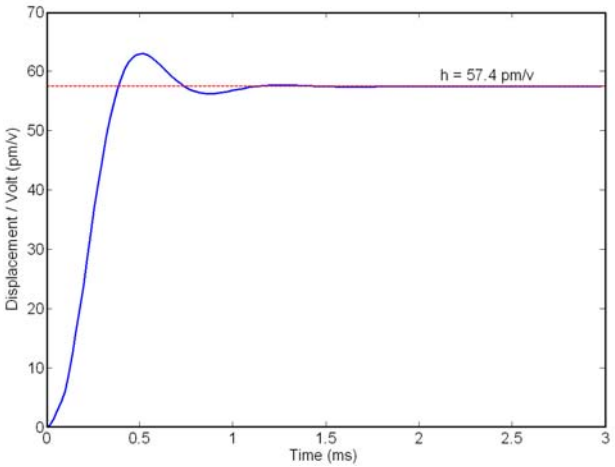

Fig. 7. Response of PPLN to the unit step input voltage at test point.

VIII. Acknowledgements

The materials presented here are based upon work supported by the National Science Foundation (CAREER Grant No. CMMI-0238987, and MRI Program Grant No. CMMI-0619739). Any opinions, findings, and conclusions or recommendations expressed in this material are those of the authors and do not necessarily reflect the views of the National Science Foundation.

References

[1] E. Kouno, "Fast response piezoelectric actuator for servo correction of systematic errors in precision machining," *CIRP Annals* 33 (1984) 369-372.

[2] WP. Mason, "Piezoelectricity, its history and applications," *Journal of Acoustical Society of America*, 70 (1981) 1561-1566.

[3] D. Berlincourt, "Piezoelectric ceramics: characteristics and applications," *Journal of Acoustical Society of America* 70 (1981) 1586-1595.

[4] A. M. Flynn, L. S. Tavrow, S. F. Bart, R. A. Brooks, D. J. Ehrlich, K. R. Udayakumar, and L. E. Cross, "Piezoelectric micromotors for microrobots," *Journal of Microelectromechanical Systems* 1 (1992) 44-51.

[5] P. Lugienbuhl, S. D. Collins, G. A. Racine, M. A. Gretillat, N. F. D. Rooij, K. G. Brooks, and N. Setter, "Ultrasons flexural lamb-wave actuators based on PZT thin film," *Sensors and Actuators A* 64 (1998) 41-49.

[6] A. Gruverman and A. Kholkin, "Nanoscale ferroelectrics: processing, characterization and future trends," *Reports on Progress in Physics* 69 (2006) 2443-74.

[7] F. Felten, G. Schneider, J. Saldana, and S. Kalinin, "Modeling and measurement of surface displacement in BaTiO3 bulk material in piezoresponse force microscopy," *Journal of Applied Physics* 96(1) (2004) 563-68.

[8] P. Guthner and K. Dransfeld, "Local poling of ferroelectric polymers by scanning force microscopy," *Applied Physics Letters* 61 (92) 1137-39.

[9] A. Gruverman, H. Tokumoto, A. S. Prakash, S. Aggarwal, B. Yang, M. Wuttig, R. Ramesh, and O. Auciello, "Nanoscale imaging of domain dynamics and retention in ferroelectric thin film," *Applied Physics Letters* 71 (1997) 3492-94.

[10] T. Hidaka, M. Maruyama, M. Saitoh, N. Mikoshiba, M. Shimizu, T. Shiosaki, L. A. Wills, R. Hiskes, S. A. Dicarolis, and J. Amano, "Formation and observation of 50 nm polarized domains in Pb Zr_{1-x} $TixO_3$ thin films using scanning probe microscope," *Applied Physics Letters* 68 (1996) 2358-59.

[11] S. Kalinin, E. Karapetian, and M. Kachanov, "Nanoelectromechanics of piezoresponse force microscopy," *Physical Review B* 70 (2004) 184101(1-24).

[12] S. Hong, J. Woo, H. Shin, J. Joen, Y. Pak, E. Colla, N. Settar, E. Kim, and K. No, "Principle of ferroelectric domain imaging using atomic force microscopy," *Journal of Applied Physics* 89(2) (2001) 1377-1386.

[13] S. Jesse, A. P. Baddorf, S. Kalinin, "Dynamic behavior in piezoresponse force microscopy," *Nanotechnology* 17 (2006) 1615-1628.

[14] A. Salehi-Khojin, N. Jalili, and S. N. Mahmoodi, "Vibration Analysis of Vector Piezoresponse Force Microscopy with Coupled Flexural-Longitudinal and Lateral-Torsional Motions", *Journal of Sound and Vibration*, in-print (2009) 1-19.

[15] S. Kalinin and D. Bonnell, "Imaging mechanism of piezoresponse force microscopy of ferroelectric surfaces," *Physical Review B* 65 (2002) 125408(1-11).

[16] L. E. Myers and W. R. Bosenberg, "Periodically poled lithium niobate and quasi-phase-matched optical parametric oscillators," *IEEE Journal of Quantum Electronics* 33(10) (1997) 1663-1672.

[17] J. Matyas, "Random optimization," *Automation and Remote Control* 22 (1995) 246-253.